Exposition of Noise Fraction Adjustments for Integrated Noise Modeling of Rotary-Wing Vehicles

Stephen A. Rizzi[1] and Stefan J. Letica[2]
NASA Langley Research Center, Hampton, VA 23681, USA

The noise fraction adjustment is one of several adjustments to noise-power-distance data that are used to estimate sound exposure in integrated noise modeling. The noise fraction adjustment relates the sound exposure due to an infinitely long flyover to that generated by a finite segment. This paper elucidates the origins and derivation of this adjustment. The paper also offers alternative formulations of the noise fraction adjustment that may be better suited for different helicopter and urban air mobility vehicles and their different operational modes, i.e., departure, overflight, and approach. These alternatives can alter noise fraction estimates by several decibels.

Nomenclature

E	=	total sound exposure, Pa^2-s
F	=	noise fraction
L	=	sound pressure level, dB
L_E	=	sound exposure level, dB
L_{EPN}	=	effective perceived noise level, EPNdB
L_{PNT}	=	tone-corrected perceived noise level, PNdB
$\mathcal{L}$	=	finite flight path segment length, ft (m)
p^2	=	mean square pressure, Pa^2
PCPA	=	perpendicular closest point of approach
s	=	distance between flight path and observer at PCPA, ft (m)
t	=	time, s
τ	=	time difference between aircraft position and PCPA, s
V	=	airspeed, ft/s (m/s)
x	=	observer location, ft (m)

Subscripts

A	=	A-weighted
mx	=	maximum value
o	=	reference value
v	=	arbitrary flight path segment

I. Introduction

THE integrated noise modeling method, as standardized for fixed-wing air vehicles in ICAO Doc. 9911 [1] and as implemented in the FAA Aviation Environmental Design Tool (AEDT) [2], is used to estimate community noise exposure in the vicinity of airports. The AEDT also applies a similar methodology in the analysis of noise exposure due to helicopter operations. Recent work by Rizzi and Rafaelof [3] using AEDT demonstrated the modeling of rotary-wing vehicles, specifically types being developed for urban air mobility (UAM) operations, in both AEDT fixed-wing and helicopter modes, irrespective of their actual vehicle architectures. Subsequent work by the authors [4] focused on investigating best practices for modeling UAM vehicle noise using AEDT in fixed-wing and helicopter modes. A comparative study between simulation, using the NASA Aircraft Noise Prediction Program 2 (ANOPP2) [5] Mission Analysis Tool (AMAT), and integrated noise modeling, using the FAA AEDT, was conducted for the

[1] Senior Researcher for Aeroacoustics, Aeroacoustics Branch, stephen.a.rizzi@nasa.gov, AIAA Fellow
[2] Research Engineer, Aeroacoustics Branch, stefan.j.letica@nasa.gov

NASA Quadrotor reference vehicle [6]. It was found that the differences between AEDT analysis modes were due to several factors. These included i) the lack of an explicit lateral directivity adjustment in AEDT fixed-wing mode, ii) a limitation in the number of unique helicopter mode noise-power-distance (NPD) data that could be used in departure, approach, and overflight, and iii) apparent differences in the noise fraction adjustment between fixed-wing and helicopter modes in the landing and takeoff area. It should be noted that the noise fraction adjustment in Doc. 9911 was developed to represent the sound pressure level time history for large, jet-powered commercial transports [7], so the applicability of the adjustment to UAM vehicles is unknown.

The purpose of this paper is to elucidate the formulation and function of the noise fraction adjustment as currently recommended in Doc. 9911. To that end, a short review of the integrated noise modeling method is offered to provide context for the noise fraction adjustment amongst several other adjustments used for noise exposure estimation. Simple examples of departure, overflight, and approach operations are used to demonstrate that exposure estimates in AEDT fixed-wing and helicopter modes can be made practically equivalent by modeling operations in a way that minimizes differences between the various adjustments. Following that, a thorough treatment of the noise fraction adjustment is made to explain both its origin and its application. Alternative formulations to that recommended in Doc. 9911 are derived to explore the possibility of selecting different forms for different aircraft and operations. Finally, the fitness of each of several formulations to different helicopters and UAM concept vehicles is assessed using NPD data derived from helicopter acoustic flight tests [8-10] and mid-fidelity analyses [11], respectively. This work is aligned with a recommendation of a recent white paper [12] that "*Research be conducted to more fully explore limitations in methods for assessing community noise impact of UAM vehicles in their operational environments, and to generate a software development plan that addresses the limitations of current models over time*."

II. Review of Integrated Noise Modeling

This section reviews the contemporary integrated noise modeling method, i.e., using flight path segmentation, for estimation of sound exposure at a set of ground observers. It discusses differences between modeling the aircraft as fixed-wing and helicopter types, starting with the NPD data that serve as input to those analyses.

A. Noise-Power-Distance Data

NPD data express measures of noise at a ground observer as a function of a noise-related engine power parameter and the slant distance between the source and ground observer. The noise-related engine power parameter specified in fixed-wing NPD data is the corrected net thrust per engine, i.e., the net thrust referenced to standard air pressure at mean sea level. The noise-related power parameter specified in helicopter NPD data is replaced by the operational mode, e.g., approach at constant speed. The noise measures correspond to an infinitely long, straight-line flight trajectory under steady conditions, at a specified reference speed, atmospheric condition, and configuration, and are provided over a range of power levels/operational modes and reference distances. NPD measures include maximum and time-integrated (exposure) noise metrics. Maximum metrics include the maximum A-weighted sound pressure level (L_{Amx}) and the maximum tone-corrected perceived noise level (L_{PNTmx}). Sound exposure metrics include the A-weighted sound exposure level (L_{AE}) and the effective perceived noise level (L_{EPN}). As will be shown in Section III.A, both maximum level and exposure metrics are needed to estimate noise exposure when using (finite) flight path segmentation.

The NPD data are provided by original equipment manufacturers. For fixed-wing aircraft, SAE-AIR-1845A [13] provides standardized methods to derive NPD data from measured flyover noise levels and known engine and flight conditions. There is no standard for calculating helicopter NPD data.

In some cases, sets of manufacturer-provided NPD data may lack one or more maximum level metrics. These missing data can be approximated by an empirical method discussed in Section III A.3.

B. Segmentation Method

The internationally recommended segmentation modeling method for fixed-wing aircraft is detailed in ICAO Doc 9911 [1] (see also ECAC.CEAC Doc 29 [14]). In this approach, the flight path is divided into a contiguous set of straight-line segments of finite length. The noise exposure at each ground observer is computed by summing the noise exposure from all flight path segments, and the maximum level may be emitted from a segment other than the closest segment.

Exposure noise metrics are calculated at each segment's perpendicular closest point of approach (PCPA), or slant range, described further in Section III.A, by interpolating/extrapolating the NPD data between power settings and between reference distances. For fixed-wing aircraft, noise exposure metrics are calculated by interpolating and/or extrapolating the NPD data between power settings and between reference distances. Although helicopters are not addressed by Doc 9911 and Doc 29, they are included in some computer implementations, notably the AEDT

helicopter mode. The AEDT interpolates/extrapolates helicopter NPD data between reference distances only, and not between operational modes.

After the NPD data are interpolated for each segment of the flight path, several adjustments must be made to account for various factors that determine the sound exposure at each observer. All adjustments for sound exposure estimates due to a single path segment *v* of a flight operation are given for fixed-wing aircraft as:

$$10\log_{10}\left(E_v\right) = L_{E,P,d-ADJ} + F_{ADJ} + DUR_{ADJ} - LA_{ADJ} + TR_{ADJ} + DIR_{ADJ} \tag{1}$$

and for helicopters as:

$$10\log_{10}\left(E_v\right) = L_{E,P,d-ADJ} + F_{ADJ} + DUR_{ADJ} - LA_{ADJ} + MN_{ADJ} + LD_{ADJ} \tag{2}$$

in which

$L_{E,P,d\text{-}ADJ}$ Sound exposure, L_{AE} or L_{EPN}, in dB, interpolated for power P (fixed-wing only) and slant range s (both fixed-wing and helicopter) from the receptor to the perpendicular closest point of approach (PCPA) on the flight path segment or extended flight path segment, and adjusted for atmospheric absorption and acoustic impedance (to account for differences between the reference-day condition associated with the NPD data and that of the particular study).

F_{ADJ} Noise fraction adjustment, in dB (see Section III)

DUR_{ADJ} Duration adjustment = 10 $\log_{10}[V_0/V]$, in dB, in which V_0 is the reference speed for the operation and V is the segment speed. The reference speed may be different for helicopter departure, overflight, and approach operations, but is 160 kts for all fixed-wing operations.

LA_{ADJ} Lateral attenuation adjustment, in dB

TR_{ADJ} Thrust reverser adjustment, in dB (fixed-wing only, not currently implemented in Doc 9911)

DIR_{ADJ} Directivity adjustment, in dB, (fixed-wing only, applied only if segment is part of takeoff ground roll)

MN_{ADJ} Advancing tip Mach number adjustment, in dB (helicopters in level flight only)

LD_{ADJ} Lateral directivity adjustment, in dB (helicopters only)

Additional information on each of the adjustments can be found in Ref. [2].

This work is focused on F_{ADJ}, the noise fraction adjustment. NPD data measurements (or simulations) are provided assuming an infinitely long flyover. As each segment is treated as a finite part of the infinitely long flyover used in the generation of the NPD data, an adjustment must be made to the interpolated sound exposure to determine how much sound exposure is produced by that portion of the infinite flyover. A semi-empirical relationship called the noise (or energy) fraction is used to apportion the noise exposure data of the infinite segment to each finite segment. The noise fraction adjustment is discussed in detail in Section III.

C. Simplified Departure, Overflight, and Approach Operations

Analyses of three simplified operations (departure, overflight, and approach) were performed in the AEDT to demonstrate that the adjustments in Eqs. (1) and (2) can either be made the same or eliminated to achieve practically identical noise exposure estimates when making comparisons between modeling aircraft as fixed-wing and helicopters, provided that NPD data are available to do so. Simplified operations versus more practical operations were modeled primarily to avoid the AEDT limitation of allowing only one operating state (determined by a combination of airspeed and climb angle) to represent a departure at constant speed (procedural operating mode D) and another to represent an approach at constant speed (procedural operating mode A). Furthermore, fixed-point flight profiles were used when modeling the aircraft in AEDT fixed-wing mode [15] allowing identical operating states for fixed-wing and helicopter analyses without use of a nonexistent UAM performance model.

To the greatest extent possible, the same operating conditions for fixed-wing and helicopter were specified for departure, overflight, and approach operations. These are summarized in Table 1 for fixed-wing mode and in Table 2 for helicopter mode. Fixed-wing and helicopter NPD data used were taken from those generated in Ref. [11] and represented 20 kt, 10° climb for all departure steps, 90 kt, 0° climb for all overflight steps, and 20 kt, -10° climb for all approach steps.

Table 1: Fixed-point flight profile data for modeling simplified operations in fixed-wing mode.

Operation Type	Distance Along Track (ft)	Altitude† (ft)	Speed (kts)
Departure	0	15	20
	15000	2660	20
	15001	2660	20
Overflight	0	1000	90
	31680	1000	90
Approach	0	2660	20
	1	2660	20
	15001	15	20

† Above field elevation (departure and approach), mean sea level (overflight)

Table 2: Operational procedural steps for modeling simplified operations in helicopter mode.

Operation Type	Operational Procedural Step [AEDT]	Segment Length (ft)	Ending Altitude† (ft)	Ending Speed (kts)	Duration (s)
Departure	G	-	0	-	0.001
	H	-	0	-	0.001
	V	-	15	-	0.001
	E	1	15	20	-
	D	14999	2660	20	-
	L	1	2660	20	-
Overflight	S	-	1000	90	-
	L	31680	1000	90	-
Approach	S	-	2660	20	-
	L	1	2660	20	-
	A	14999	15	20	-
	B	1	15	0	-
	Y	-	0	0	0.001
	H	-	0	-	0.001
	G	-	0	-	0.001

† Above field elevation (departure and approach), mean sea level (overflight)

With respect to Eq. (1), fixed-wing types were specified as propeller-driven aircraft to set i) the thrust reverser adjustment to zero and ii) the engine installation portion of the lateral attenuation adjustment to zero. The remaining portions of the lateral attenuation adjustment are ground reflection and refraction effects, which are common to fixed-wing and helicopter analyses. The special cases of noise fraction adjustments for receptors before the start of takeoff roll and receptors after the end of landing roll (to be discussed in Section III.5) and for the takeoff roll directivity adjustment (DIR_{ADJ}), all particular to fixed-wing mode, were avoided by not including takeoff and landing rolls. With respect to Eq. (2), the advancing tip Mach number adjustment was eliminated by setting the "B" coefficients to zero [2] and the lateral directivity adjustment was eliminated by setting the lateral (±45°) NPD data to be identical to the centerline NPD data. Further, the noise exposure from static helicopter modes (G, H, V, Y) [2], for which there is no fixed-wing equivalent, were minimized by specifying a minimal duration for each. These modes are required according to the mandatory procedural step sequence for helicopters. More general practices for modeling UAM vehicles in AEDT fixed-wing and helicopter modes can be found in Refs. [3,15].

Sound exposure estimates for each operation are shown in Figure 1. In all cases, the differences between fixed-wing and helicopter mode results were negligible, with a maximum average difference of < 0.004 dBA.

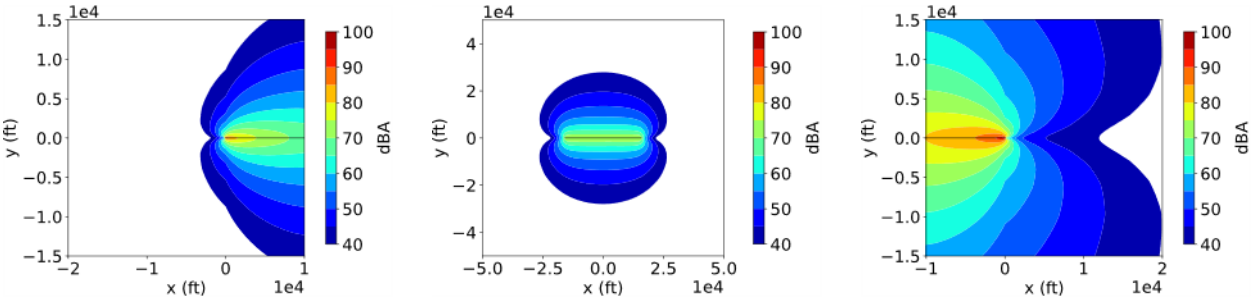

Figure 1: Sound exposure estimates of NASA Quadrotor reference vehicle for simplified departure (left, starting at x = 0), overflight (center), and approach (right, ending at x = 0) operations.
The black line indicates the ground track.

III. Noise Fraction Adjustment

The noise fraction represents the fractional relationship between the sound exposure associated with an infinitely long flyover and that associated with a finite segment of that flyover. It can be written as

$$F_{12} = E_{12} / E_{\infty} \tag{3}$$

in which E_{12} is the sound exposure associated with the finite flight path segment, and E_{∞} is the sound exposure associated with the infinite flight path. The noise fraction for a given flight path segment is based on both the geometrical relationship between the segment and the observer (J. Olmstead, personal communication, Oct. 30, 1994), and the sound exposure level and maximum sound level interpolated from the NPD data at the observer location (J. Olmstead, personal communication, Dec. 14, 1998). The derivation parallels (J. Olmstead, personal communication, Oct. 30, 1994 and Dec. 14, 1998) with a few extra steps to assist the reader. In the following, E is assumed to be A-weighted.

A. Fourth-Power Model

Figure 2 shows a straight, level flyover of a vehicle on a finite flight path segment extending from point P_1 to point P_2 within an infinite flight path extending to $\pm\infty$. An observer is positioned at location x, q_1 is the distance from P_1 to the perpendicular closest point of approach (PCPA), and the time difference between them is $\tau_1 = t_1 - t_s$. For a constant segment flyover speed, V, q_1 is given by:

$$q_1 = -V\tau_1 \quad \text{for } q_1 > 0 \ . \tag{4}$$

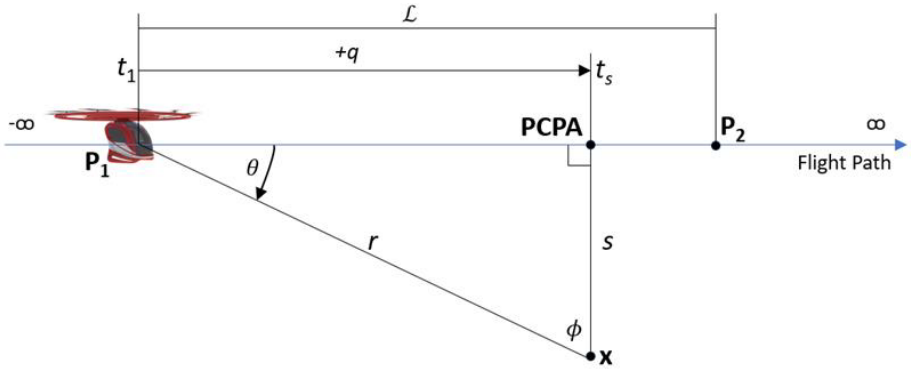

Figure 2: Geometrical relationship of finite segment $\overline{P_1P_2}$ to observer x.

The total sound exposure associated with an arbitrary flight path segment and an arbitrary observer is:

$$E_v = \int_{\tau_1}^{\tau_2} p^2(\tau)\, d\tau \tag{5}$$

in which $p^2(\tau)$ is the mean square sound pressure at the observer at time τ. The 4th-power 90° dipole model of sound radiation uses the following formulation of $p^2(\tau)$:

$$p^2(\tau) = p_s^2 \left(\frac{s^2}{r^2} \right) \sin^2 \theta \tag{6}$$

in which p_s^2 is the mean square sound pressure at the observer when the vehicle is at the PCPA, s is the distance from the flight path to the observer (or from the extended flight path to the observer for $\mathcal{L} < q_1 < 0$) at the PCPA, and r is the distance from point P_1 to the observer. Note that r and θ are functions of τ. The assumption that $p^2(\tau)$ is a maximum when the vehicle is at the PCPA requires that the source noise directivity be a maximum at $\theta = 90°$, i.e.,

$$\max\left(p^2(\tau) \right) = p_s^2 \ . \tag{7}$$

The quantity (s^2 / r^2) represents spherical spreading loss and the 90° dipole expression $\sin^2 \theta$ approximates other physical phenomena including atmospheric attenuation, source directivity, Doppler shift, etc. (J. Olmstead, personal communication, Oct. 30, 1994).

1. *Behavior of the 4th-Power Model*

From Figure 2, it is seen that $\sin^2 \theta = s^2 / r^2$. This reduces Eq. (6) to:

$$p^2(\tau) = p_s^2 \left(\frac{s^4}{r^4} \right) \tag{8}$$

in which the mean square pressure is seen to decrease as $\sim 1/r^4$ (hence "4th-power model"). The maximum A-weighted sound pressure level, L_{Amx}, is defined as:

$$L_{Amx} = 10 \log_{10} \left[\frac{\max\left(p^2(\tau) \right)}{p_o^2} \right] \tag{9}$$

in which the reference pressure is $p_o = 20$ μPa. Eq. (8) can be written in terms of the A-weighted sound pressure level giving:

$$L_A(\tau) = L_{Amx} + 10 \log_{10} \left[\frac{s^4}{r^4(\tau)} \right] . \tag{10}$$

Figure 3 shows how the sound radiation model predicts the sound pressure level time history for different values of s and V. This model was shown to agree well with measured data [7].

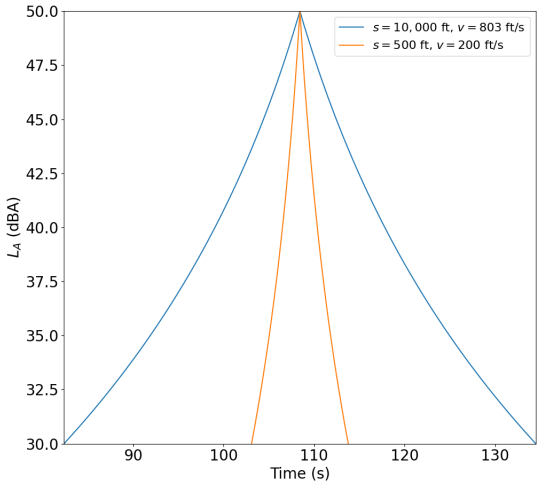

Figure 3: L_A time histories constructed using Eq. (10).

2. *Noise Fraction Based on Geometry Only*

Recognizing from Figure 2 that:

$$r^2 = s^2 + q_1^2 = s^2 + (-V\tau)^2 , \tag{11}$$

then

$$\frac{r^2}{s^2} = 1 + \left(\frac{V\tau}{s}\right)^2 \tag{12}$$

and

$$\sin^2\theta = s^2/r^2 = 1\Big/1 + \left(\frac{V\tau}{s}\right)^2 . \tag{13}$$

Eq. (5) can be rewritten as:

$$E_v = p_s^2 \frac{s}{V}\int_{\alpha_1}^{\alpha_2} \frac{1}{\left(1+\alpha^2\right)^2}\, d\alpha \tag{14}$$

using Eq. (13) and the substitution:

$$\alpha = \frac{V\tau}{s}, \quad d\alpha = \frac{V}{s} d\tau \ . \tag{15}$$

The solution to Eq. (14) is given by:

$$E_v = p_s^2 \frac{s}{V}\frac{1}{2}\left[\frac{\alpha}{1+\alpha^2} + \tan^{-1}\alpha\right]\Bigg|_{\alpha_1}^{\alpha_2} . \tag{16}$$

Its evaluation on an arbitrary, finite interval from α_1 to α_2 gives the numerator of Eq. (3) as:

$$E_{12} = p_s^2 \frac{s}{V}\frac{1}{2}\left[\frac{\alpha_2}{1+\alpha_2^2} + \tan^{-1}\alpha_2 - \frac{\alpha_1}{1+\alpha_1^2} - \tan^{-1}\alpha_1\right] \tag{17}$$

and its evaluation on the infinite interval from $\alpha_1 = -\infty$ to $\alpha_2 = +\infty$ gives the denominator of Eq. (3) as:

$$E_\infty = p_s^2 \frac{s}{V}\frac{\pi}{2} \ . \tag{18}$$

From Eq. (3), the noise fraction is:

$$F_{12} = \frac{E_{12}}{E_\infty} = \frac{1}{\pi}\left[\frac{\alpha_2}{1+\alpha_2^2} + \tan^{-1}\alpha_2 - \frac{\alpha_1}{1+\alpha_1^2} - \tan^{-1}\alpha_1\right] \tag{19}$$

with

$$\alpha_1 = -\frac{q_1}{s}, \quad \alpha_2 = \frac{\mathcal{L} - q_1}{s} \ . \tag{20}$$

Note that Eq. (19) consists solely of terms related to the geometry of the flight path and the observer. The noise fraction adjustment, expressed in dB, is given by:

$$F_{ADJ} = 10\log_{10}(F_{12}) \ . \tag{21}$$

3. Relationship Between Sound Exposure Level and Maximum Level

The A-weighted sound exposure level, L_{AE}, is defined as:

$$L_{AE} = 10\log_{10}\left[\frac{E_v}{p_o^2 t_o}\right] \tag{22}$$

in which p_o = 20 μPa and t_o = 1 s are the reference pressure and time, respectively. In essence, L_{AE} represents the total sound energy of the event "compressed" into the reference time. An "effective" value of the mean squared pressure, p_{eff}^2, represents a value that produces the same sound exposure level as the original event when applied at a constant level over a period of 1 s. In other words, Eq. (5) gives:

$$E_v = \int_{\tau_1}^{\tau_2} p^2(\tau)\, d\tau = p_{eff}^2 t_o \ . \tag{23}$$

Consider the sound pressure time history $p^2(\tau)$ for an idealized flyover shown by the blue triangle in Figure 4. The area under the triangle represents the total sound exposure due to the flyover event. Eq. (23) states that the area under the dark blue triangle is equal to the area of the light blue rectangle.

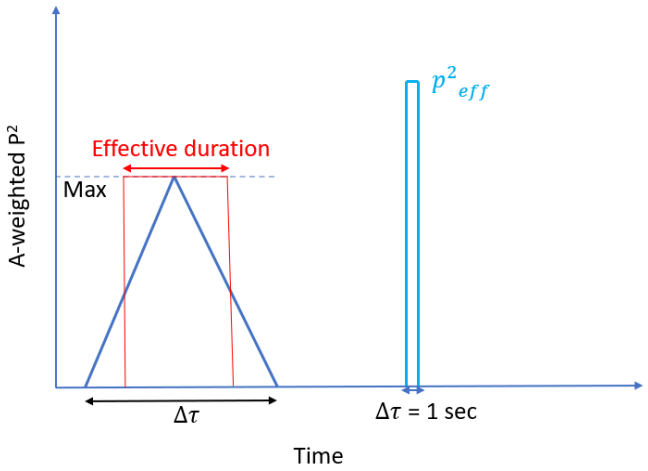

Figure 4: Relationship between L_{AE}, L_{Amx}, and Δt_{eff}.

A useful means of expressing the relationship between L_{AE} and L_{Amx} is through the "effective duration" Δt_{eff} (J. Olmstead, personal communication, Oct. 30, 1994), shown by the red rectangle in Figure 4. Here, the L_{AE} associated with the red rectangle is the same as both the blue triangle and blue rectangle. Mathematically, the total sound exposure represented by the red rectangle is:

$$E_v = \max\left(p^2(\tau)\right)\Delta t_{eff} \quad \text{or} \quad \Delta t_{eff} = \frac{E_v}{\max\left(p^2(\tau)\right)} \,. \tag{24}$$

Adding a unity factor on the right-hand side and converting to dB referenced to $t_o = 1$ s gives:

$$\begin{aligned} 10\log_{10}\left[\frac{\Delta t_{eff}}{t_o}\right] &= 10\log_{10}\left[\frac{E_v}{\max\left(p^2(\tau)\right)}\frac{1}{t_o}\frac{p_o^2}{p_o^2}\right] \\ &= 10\log_{10}\left[\frac{E_v}{p_o^2 t_o}\right] - 10\log_{10}\left[\frac{\max\left(p^2(\tau)\right)}{p_o^2}\right] = L_{AE} - L_{Amx} \end{aligned} \,. \tag{25}$$

Thus, we find that the relationship between L_{AE} and L_{Amx} can be represented by Δt_{eff}, a value with units of time. This relationship is important because it identifies the key principles by which sound energy is incorporated into the geometric noise fraction Eq. (19). These two quantities are those typically provided by aircraft manufacturers and are key to the noise prediction methodology.

Where's My L_{Amx}?

Several fixed-wing aircraft and nearly all helicopters in the AEDT aircraft noise and performance (ANP) database lack maximum noise level (L_{Amx} and L_{PNTmx}) NPD data. Although it is alluded to in the context of the recommended method for aircraft substitution, there is no explicit provision for making up for the lack of those data in Doc 9911 [1]. The provision in AEDT for doing so approximates maximum noise level data using empirical equations as a function of distance and L_{AE}. The approximation was developed from statistical analysis of NPD data for aircraft in which all four NPD metrics exist. Given that nearly all helicopters lack the four NPD metrics, it is surmised that the approximation is based either solely or largely on data from fixed-wing aircraft. Nevertheless, the same approximation is applied to both helicopters and fixed-wing aircraft. The approximation is given as:

$$L_{Amx} = L_{AE} - 7.19 - 7.73\log_{10}\left(\frac{s}{1000}\right) \tag{26}$$

in which the distance at the PCPA s is given in ft. Under this approximation, the effective duration is given by:

$$\Delta t_{eff} = 10^{\frac{\left(7.19+7.73\log_{10}\left(\frac{s}{1000}\right)\right)}{10}} \quad . \tag{27}$$

In practice, Eq. (26) is used to approximate L_{Amx} at all ten NPD distances preceding its interpolation to the observer distance.

4. Noise Fraction Based on Geometry and Sound Energy

Olmstead (J. Olmstead, personal communication, Dec. 14, 1998) recognized a deficiency in the noise fraction that is based solely on geometry. In demonstrating this, he considered the case of a finite segment of 270.05 ft flown at the reference speed of 160 kts [1]. This results in a flight time of $\Delta\tau$ = 1 s. When the PCPA lies somewhere along this flight segment, L_{AE} and L_{Amx} should be equal according to Eq. (25). However, Olmstead showed that the 4th-power model given by Eq. (19) underpredicts the value of L_{AE} relative to the known value of L_{Amx} at all observer distances, with the discrepancy growing larger with increasing distance. Thus, the purely geometric 4th-power model does not adequately capture all the physics of sound exposure from a flight path segment, and the sound energy associated with the noise exposure and maximum level must both be accounted for in the noise fraction.

To incorporate the known values of L_{AE} and L_{Amx} into the geometry noise fraction Eq. (19), the following relationship based on Eqs. (22) and (9) must hold [2]:

$$L_{AE,0} - L_{Amx} = 10\log_{10}\left[\frac{V}{V_o}\frac{E_\infty}{p_o^2 t_o}\right] - 10\log_{10}\left[\frac{\max\left(p^2(\tau)\right)}{p_o^2}\right] \tag{28}$$

in which $L_{AE,0}$ and L_{Amx} represent the NPD data interpolated for distance with reference speed V_o. Note that L_{Amx} is the interpolated maximum level at the PCPA on the extended track, not the interpolated maximum level at the closest point of approach. The factor of V/V_o is included in the L_{AE} term to correct the sound exposure level from the segment airspeed, V, to the reference airspeed of the NPD, V_o. The NPD data represent an infinite flyover, so E_∞ is used to represent the sound exposure. Substituting Eqs. (7) and (18) from the 4th-power model into Eq. (28) yields:

$$L_{AE,0} - L_{Amx} = 10\log_{10}\left[\frac{V}{V_o}\frac{p_s^2\frac{s}{V}\frac{\pi}{2}}{p_o^2 t_o}\right] - 10\log_{10}\left[\frac{p_s^2}{p_o^2}\right] \tag{29}$$

or

$$10^{\frac{L_{AE,0}-L_{Amx}}{10}} = \frac{\pi}{2}\frac{s}{V_o t_o} \quad . \tag{30}$$

From Eq. (25), the left-hand side of Eq. (30) is the effective duration $\Delta t_{eff}/t_o$. Solving for s yields:

$$s = \frac{2}{\pi} t_o V_o 10^{\frac{L_{AE,0}-L_{Amx}}{10}} \quad . \tag{31}$$

This s represents the slant distance at which calculation of the noise fraction correctly relates the measured energy values in the NPD database. As it is essentially a scaling factor, it is called the "scaled distance," s_L. Eq. (31) may be rewritten as:

$$s_L = s_o \frac{\Delta t_{eff}}{t_o}, \quad s_o = \frac{2}{\pi} t_o V_o \quad . \tag{32}$$

This particular form of s_o, like the form of the effective duration in Eq. (25), is a consequence of the 4th-power model. Both the scaled distance and effective duration indicate how L_{AE} and L_{Amx} are related for a given event.

Finally, Eq. (32) can be substituted into Eq. (20) to obtain α_1 and α_2 in terms of s_L giving:

$$\alpha_1 = -\frac{q_1}{s_L}, \quad \alpha_2 = \frac{\mathcal{L} - q_1}{s_L} \quad . \tag{33}$$

Eqns. (19) and (33) constitute the 4th-power noise fraction formulae that are specified in Ref. [1].

The noise fraction adjustments for the NASA Quadrotor reference vehicle for single segment departure, overflight, and approach operations are shown in Figure 5. The departure segment consists of a 20 kt, 10° climb starting at an altitude of 15 ft at x = 0, over a track length of 15 kft. The 90 kt, level overflight segment at 500 ft altitude extends

from -1000 ≤ x ≤ 1000 ft. The approach segment consists of a 20 kt, 10° descent ending at an altitude of 15 ft at x = 0, over a track length of 15 kft. All NPD data are taken from Ref. [11].

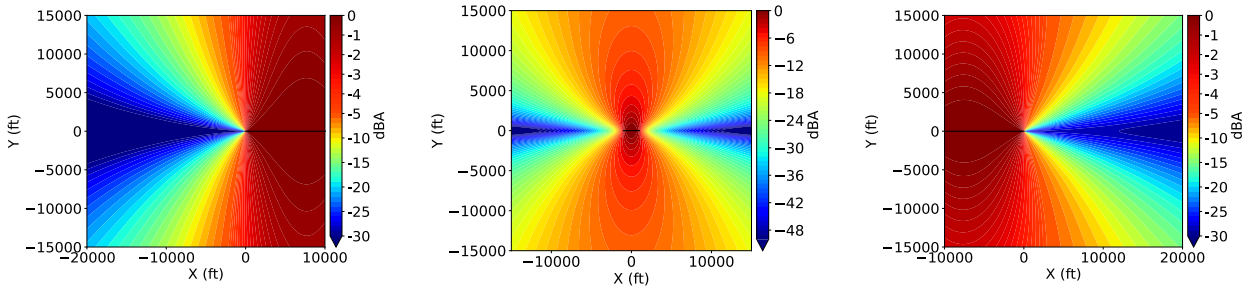

Figure 5: Noise fraction adjustment (in dBA) of NASA Quadrotor reference vehicle for departure (left), overflight (middle), and approach (right). The black line indicates the ground track.

5. Special Cases for Takeoff and Landing Ground Roll Segments

The noise fraction differs for takeoff and landing ground roll segments. In the special case of the takeoff ground roll segment, Eqs. (19) and (33) are still used, but with the caveat that, for this segment only, all observers at points for which $q_1 < 0$, i.e., observers behind the takeoff roll, are treated as $q_1 = 0$. This leads to Eqs. (19) and (33) taking new, simplified forms (for these observers only) as:

$$F_{12,d} = \frac{1}{\pi}\left[\frac{\alpha_2}{\left(1+\alpha_2^2\right)} + \tan^{-1}\left(\alpha_2\right)\right], \qquad \alpha_2 = \frac{\mathcal{L}}{s_L} \; . \tag{34}$$

Likewise, in the special case of the landing ground roll segment, all observers at points for which $q_1 > \mathcal{L}$, i.e., observers beyond the landing roll, are treated as $q_1 = \mathcal{L}$, leading to:

$$F_{12,a} = \frac{1}{\pi}\left[-\frac{\alpha_1}{\left(1+\alpha_1^2\right)} - \tan^{-1}\left(\alpha_1\right)\right], \qquad \alpha_1 = \frac{-\mathcal{L}}{s_L} \; . \tag{35}$$

There is no specific justification offered by Refs. [1,2,14] for using these forms. However, Eqs. (34) and (35) are those used in current practice when modeling vehicles as fixed-wing aircraft. This form is not used when modeling vehicles as helicopters (AEDT only), as ground roll segments cannot be used when modeling in AEDT helicopter mode. In addition, when a takeoff ground roll segment is present, it is accompanied by the takeoff roll directivity adjustment (DIR_{ADJ}).

The noise fraction adjustment for the departure with takeoff ground roll is shown in the lefthand plot in Figure 6. The noise fraction shown does not account for the takeoff ground roll directivity adjustment. The righthand plot indicates the difference between Eq. (19) using the scaled distance and Eq. (34). This special case adjustment for takeoff ground roll (x ≤ 0) replaces the large attenuation seen in Figure 5 (left) with a minimum attenuation of 3 dBA (at the origin) which slowly increases with increasing slant range.

The noise fraction adjustment for the approach with landing ground roll is shown in the lefthand plot in Figure 7. The righthand plot indicates the difference between Eq. (19) using the scaled distance and Eq. (35). As in Figure 6, the special case adjustment for landing ground roll (x ≥ 0) replaces the large attenuation seen in Figure 5 (right).

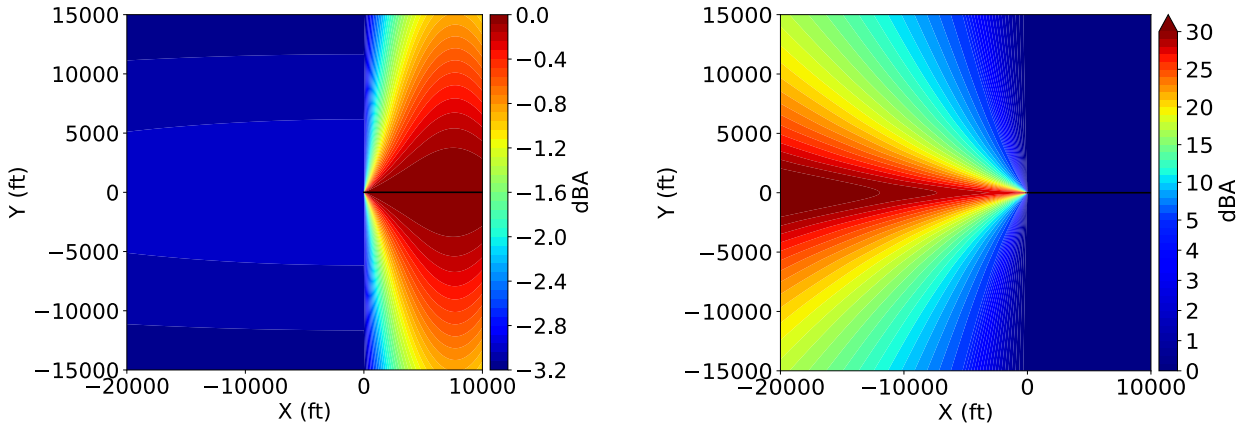

Figure 6: Special case of noise fraction adjustment (in dBA) for takeoff ground roll (without takeoff ground roll directivity adjustment) of the NASA Quadrotor reference vehicle. The black line indicates the ground track.

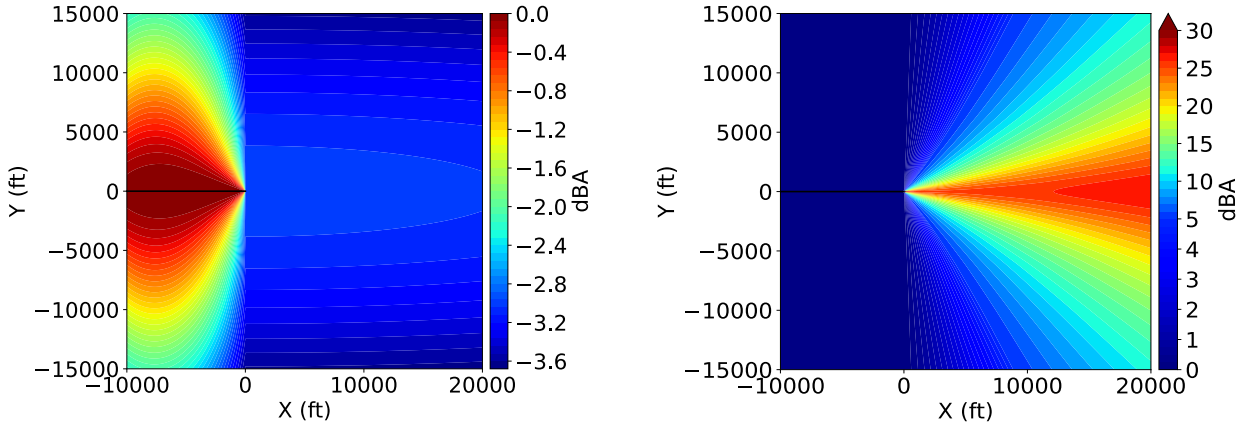

Figure 7: Special case of noise fraction adjustment (in dBA) for landing ground roll of Quadrotor reference vehicle. The black line indicates the ground track.

B. n^{th} – Power Models

Other powers of the sine-squared, 4th-power can be derived by using a different approximation for the other physical phenomena that affect sound propagation. These relationships can be summarized by writing the approximation of the physical phenomena as $\sin^{n-2}\theta$, in which n is the desired power. Figure 8 shows an example of how the chosen power affects the time history of a flyover, keeping the altitude and speed constant. Increasing the power of the model decreases the area under the sound pressure level time history curve. In other words, it decreases the predicted difference between L_{AE} and L_{Amx}, and thereby decreases the effective duration Δt_{eff}.

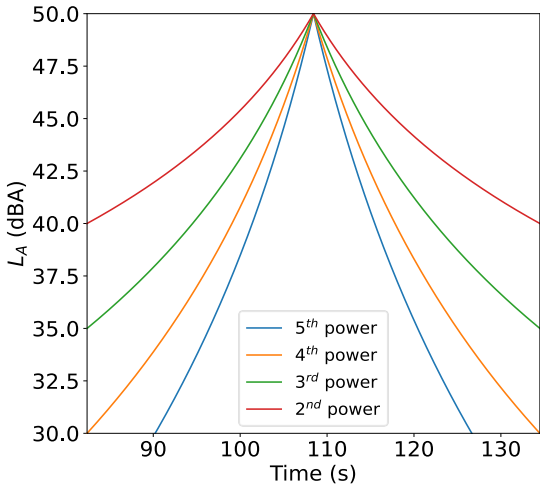

Figure 8: n[th]-power models of time history of L_A for constant speeds and altitudes.

New relationships for quantities of interest can be derived by starting with the substitution of $\sin^{n-2}\theta$ in Eq. (6) giving:

$$p^2(\tau) = p_s^2\left(\frac{s^2}{r^2}\right)\sin^{n-2}\theta = p_s^2\left(\frac{s^n}{r^n}\right) . \tag{36}$$

After some algebra, Eq. (36) can be used to rederive all the previously defined descriptive variables as:

$$E_v = p_s^2\frac{s}{V}\int_{\alpha_1}^{\alpha_2}\frac{1}{\left(1+\alpha^2\right)^{n/2}}\,d\alpha \ . \tag{37}$$

Eq. (37) is then evaluated to produce the form of F_{12} for different model powers. Similarly, Eq. (28) is evaluated with the power-specific version of E_∞ to obtain the power-specific effective duration Δt_{eff}, and s_o. These are provided in Table 3 for different model powers.

Table 3: E_∞, F_{12}, Δt_{eff}, and s_o for different model powers.

Power	E_∞	F_{12}	Δt_{eff}	s_o
2	$\pi\frac{s}{V}p_s^2$	$\frac{1}{\pi}\left[\tan^{-1}\alpha_2-\tan^{-1}\alpha_1\right]$	$\pi\frac{s}{V}$	$\frac{1}{\pi}t_oV_o$
3	$2\frac{s}{V}p_s^2$	$\frac{1}{2}\left[\frac{\alpha_2}{\sqrt{1+\alpha_2^2}}-\frac{\alpha_1}{\sqrt{1+\alpha_1^2}}\right]$	$2\frac{s}{V}$	$\frac{1}{2}t_oV_o$
4	$\frac{\pi}{2}\frac{s}{V}p_s^2$	$\frac{1}{\pi}\left[\frac{\alpha_2}{1+\alpha_2^2}-\frac{\alpha_1}{1+\alpha_1^2}+\tan^{-1}\alpha_2-\tan^{-1}\alpha_1\right]$	$\frac{\pi}{2}\frac{s}{V}$	$\frac{2}{\pi}t_oV_o$
5	$\frac{4}{3}\frac{s}{V}p_s^2$	$\frac{1}{4}\left[\frac{3\alpha_2+2\alpha_2^3}{\left(1+\alpha_2^2\right)^{3/2}}-\frac{3\alpha_1+2\alpha_1^3}{\left(1+\alpha_1^2\right)^{3/2}}\right]$	$\frac{4}{3}\frac{s}{V}$	$\frac{3}{4}t_oV_o$

There are two general forms to the solution of Eq. (37), one for even powers and one for odd powers. Each model power yields a different expression for each of the four quantities in Table 3. They also each reflect a unique implicit relationship between L_{AE} and L_{Amx}, which is most clearly seen through the effective duration Δt_{eff}.

For the level flyover scenario depicted in Figure 5 (center), the difference between the 4[th]-power model with $\Delta t_{eff} = (\pi/2)(s/V)$ and the other power models is shown in Figure 9. Differences in the noise fraction adjustment between the 4[th]- and 3[rd]-power models are generally negative and up to 12 dBA over the range of observers shown.

Small positive differences are seen along roughly 60° sidelobes from the segment endpoints. Greater negative differences of up to 24 dBA are seen between the 4th- and 2nd-power models, with small positive differences along the 60° sidelobes. Mostly positive differences of up to 12 dBA are seen between the 4th- and 5th-power models, with small negative differences along the 60° sidelobes. The difference between the 4th-power model noise fraction and that computed using Eq. (27) is shown in the lower right plot of Figure 9, where smaller positive (about 4 dBA) and negative (about 2 dBA) differences are observed compared with the differences seen between power models.

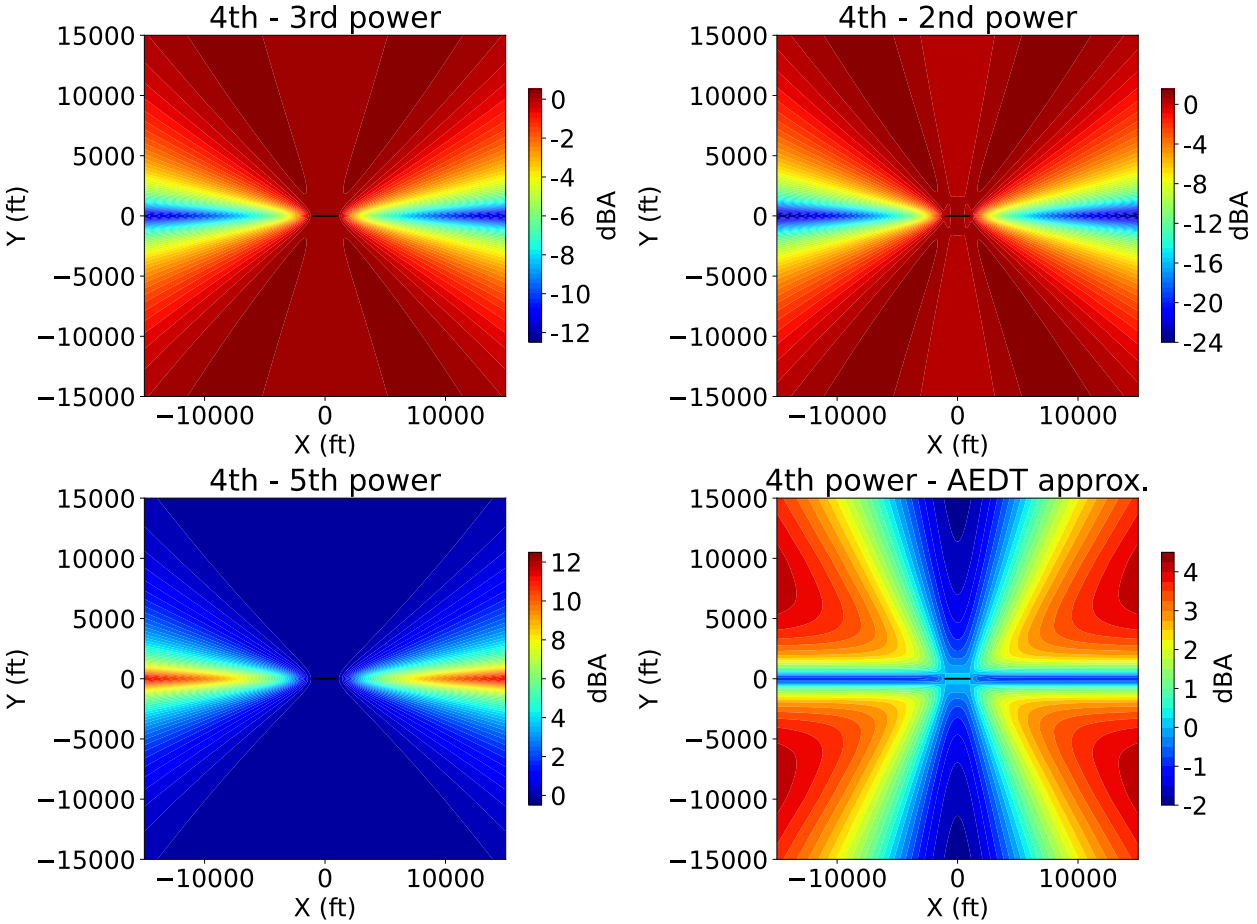

Figure 9: Difference in noise fraction adjustment (in dBA) between different power models for overflight. The black line indicates the ground track.

It should be noted that the segment reference speed, V_o, used for calculating the scaled distance in Eq. (32) must be consistent with that used for L_{AE}. This is unambiguous in the case of fixed-wing aircraft in the AEDT because all NPD data are provided for a common reference speed of 160 kts. However, in the case of helicopter mode, departure, overflight, and approach may have different reference speeds. Consequently, there is potential to provide inconsistent data in the scaled distance calculation. This can have a dramatic effect on noise exposure estimates. For example, if erroneously using a 160 kt reference speed with 20 kt L_{AE} NPD data, the noise exposure contours take on an elongated shape (compare those in Figure 10 with those in Figure 1).

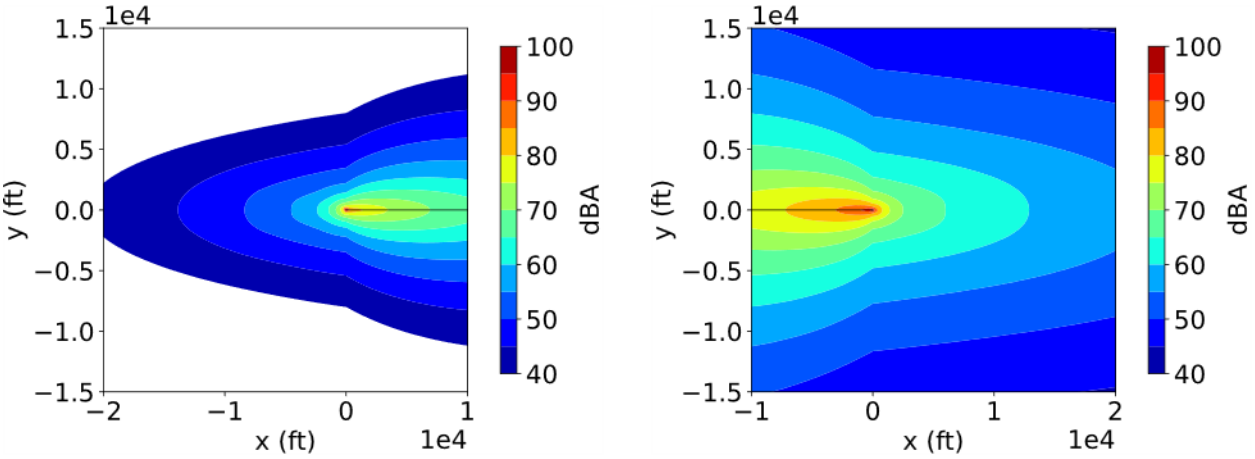

Figure 10: Example of noise exposure estimates for departure (left) and approach (right) when using reference speeds that are inconsistent with the NPD data. The black line indicates the ground track.

IV. Assessment of nth-Power Models for Helicopters and UAM Vehicles

The fitness of each nth-power model to represent the effective duration, Δt_{eff}, of different helicopters and UAM concept vehicles was assessed using NPD data derived from helicopter acoustic flight tests [8-10] and mid-fidelity analyses [11], respectively. Simulations of maximum and noise exposure metrics for departure, overflight, and approach operations were performed using the AMAT according to the method developed in Ref. [11]. Each used source noise hemispheres corresponding to a single operating condition defined by a unique pair of flight speeds and climb angles.

A. Helicopters

Source noise hemisphere data derived from helicopter flight tests were selected from a set of light helicopter weight class data, including the Robinson R44, Robinson R66, Bell 206L3, Bell 407, AS350B3, and EC130B4 [9], and medium helicopter weight class data, including the Bell 205, AW129, and S76D [8,10]. All helicopters have source noise hemispheres for approach and for constant airspeed level flight, typically between 40 kt and V_H, the maximum speed at which an aircraft can fly in level flight at maximum continuous power. V_H varies depending on helicopter model from about 130 kt to 155 kt. A limited number of departure conditions are available only for the Bell 205 and S76D. A list of conditions for which NPD data were generated is provided in Table 4.

Table 4: Helicopter operating conditions used for NPD data generation.

Vehicle	Operating Condition: Speed (kts) / Climb Angle (deg)		
	Departure	Overflight	Approach
R44	—	100 / 0	60 / -10.5
R66	—	100 / 0	60 / -9
B206L3	—	100 / 0	60 / -10.5
B407	—	100 / 0	60 / -10.5
AS350B3	—	100 / 0	60 / -10.5
EC130B4	—	100 / 0	60 / -10.5
B205	70 / 11.5	100 / 0	60 / -9
AW129	—	100 / 0	60 / -10.5
S76D	75 / 9.3	100 / 0	60 / -9

Comparisons of the effective duration computed using the NPD data per Eq. (30) and the models computed per Table 3 are summarized in Figures 11-14. The AS350B3 overflight mode L closely follows the 5th-power model with approach mode A falling somewhat below the 5th-power mode, as shown in Figure 11. The AW139, B206L3, and B407 helicopters (all omitted for brevity) exhibit similar behaviors. It should be noted that Δt_{eff} for all power models

are linear with slant range, except for the AEDT approximation model using Eq. (27). However, the effective durations from the derived NPD data are not linear with slant range and are generally more (sideways) parabolic relative to slant range. Lastly, as noted in Section III.A.3, most helicopters in the AEDT ANP database lack manufacturer-provided L_{Amx} data. In such cases, Eq. (27) is used, which forces the effective duration to follow the AEDT approximation curve with a maximal difference relative to the 4th-power model (as indicated in Figure 9). The EC130B4 (shown in Figure 12) and R66 (not shown) show a different trend, with overflight mode L more closely following the 3rd-power model and approach mode A more closely following the 4th- to 5th-power model.

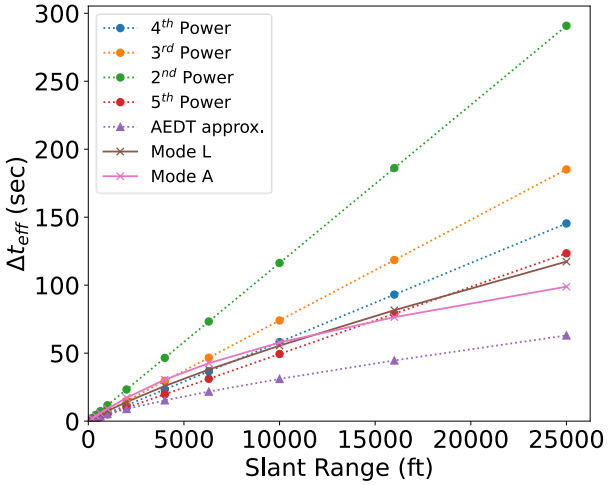

Figure 11: Comparison of effective duration of AS350B3 with model variants.

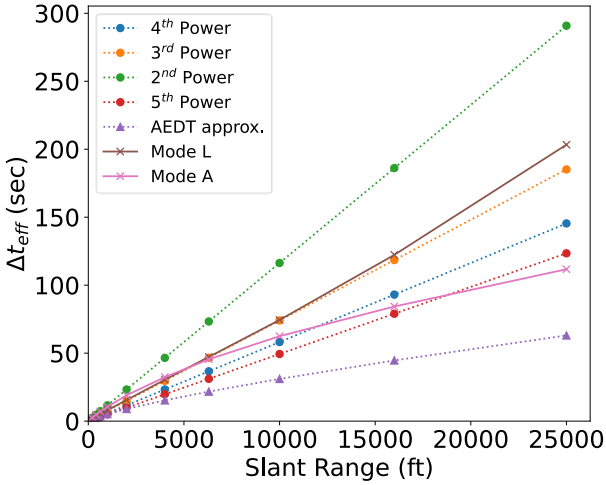

Figure 12: Comparison of effective duration of EC130B4 with model variants.

In contrast to the data shown in Figures 11 and 12, the relation of the overflight mode L to the approach mode A for the R44 helicopter is reversed, with mode A more closely following the 3rd- to 4th-power models and with mode L closest to the 5th-order model as shown in Figure 13. For the two helicopters with all three operational modes (B205 and S76D), the departure mode D most closely follows the lower-power models (2nd- to 3rd-power), with overflight mode more closely following the 3rd- to 4th-power models, and the approach mode more closely following the 4th- to 5th-power model. Data for the B205 are shown in Figure 14, with the those for the S76D omitted for brevity.

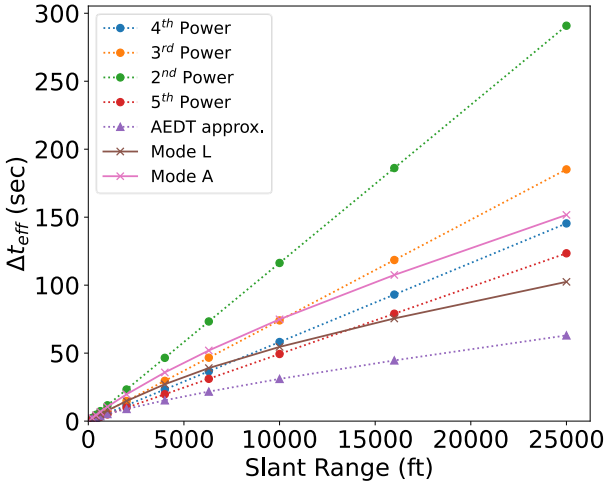

Figure 13: Comparison of effective duration of R44 with model variants.

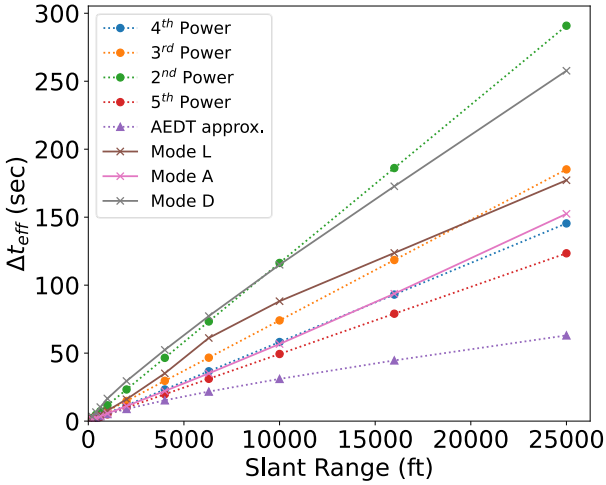

Figure 14: Comparison of effective duration of B205 with model variants.

Given the fact that there are areas of large differences in the noise fraction adjustment between different power models (Figure 9), the helicopter data suggest that use of a vehicle-specific and operational mode-specific power

model would be beneficial versus the current practice of exclusive use of the 4th-power model. Further, provision of L_{Amx} data as part of the NPD data would minimize differences with the 4th-power model, if the current practice remains in effect.

B. Urban Air Mobility Vehicles

Source noise hemisphere data [11], derived from source noise predictions of NASA UAM reference vehicles including the Quadrotor and Lift+Cruise vehicles [6], were used in simulations of departure, overflight, and approach operations. A list of conditions for which NPD data were generated is provided in Table 5.

Table 5: UAM vehicle operating conditions used for NPD data generation.

Reference Vehicle	Operating Condition: Speed (kts) / Climb Angle (deg)		
	Departure	Overflight	Approach
Quadrotor	20 / 10	90 / 0	20 / -10
Lift+Cruise	20 / 10	110 / 0	20 / -10

Comparisons of the effective duration computed using the NPD data and the models are shown in Figures 15-16 for the Quadrotor and Lift+Cruise reference vehicles, respectively.

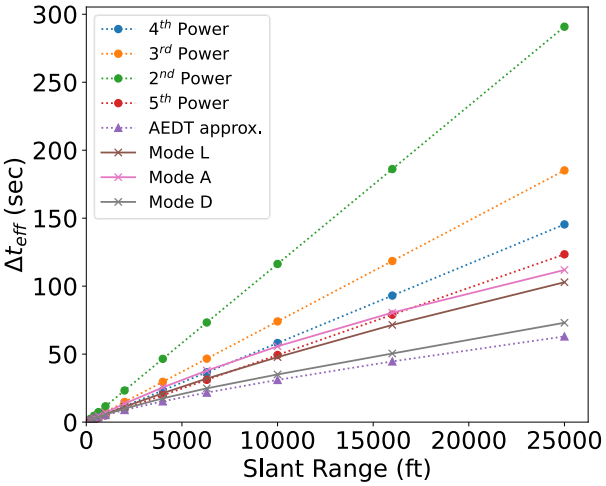

Figure 15: Comparison of effective duration of NASA Quadrotor reference vehicle with model variants.

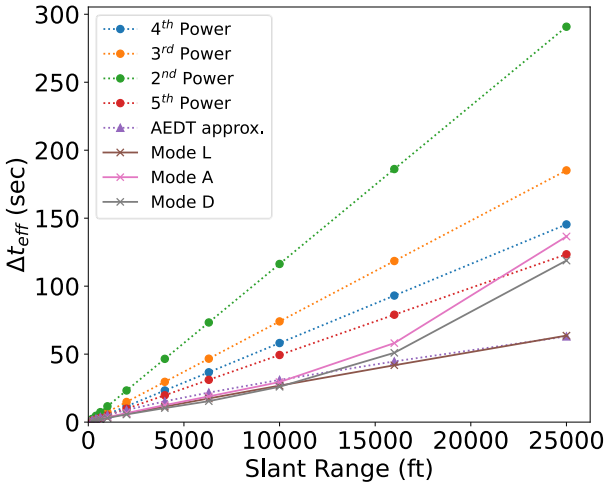

Figure 16: Comparison of effective duration of NASA Lift+Cruise reference vehicle with model variants.

The overflight mode L and approach mode A of the Quadrotor vehicle closely follow the 5th-power model, while the departure mode D closely follows the AEDT approximation. The departure mode D for the Lift+Cruise vehicle also closely follows the AEDT approximation. Below the 10k ft reference distance, the overflight mode L and approach mode A also closely follow the AEDT approximation but rise to the 5th- and 4th-order model curves, respectively, with increasing distance. This reflects an increasing difference between L_{Amx} and L_{AE} with increasing distance. Like the helicopter data, the UAM vehicle data suggest that use of a vehicle-specific and operational mode-specific power model would be beneficial versus the current practice of exclusive use of the 4th-power model.

V. Conclusions

In an effort to understand differences between integrated noise modeling using AEDT fixed-wing and helicopter modes, analyses of simplified departure, overflight, and approach operations were performed. These analyses demonstrated that near identical noise exposure estimates can be made in both modes when adjustments, including the noise fraction adjustment, are made equivalent. However, it is imperative that the reference speed used in the scaled distance calculation of the noise fraction adjustment be consistent with the speed associated with the sound exposure level metric specified as part of the NPD data. Significant distortions of noise contours occur when inconsistent data are used.

A review of the 4th-power noise fraction adjustment model showed that the noise fraction for a given flight path segment is based on both the geometrical relationship between the segment and the observer and the sound exposure level and maximum sound level interpolated from the NPD data at the observer location. Other power models, including 2nd-, 3rd-, and 5th-power models, were offered following the 4th-power model formulation. Significant differences in the noise fraction adjustment between different power models were observed in some areas. An assessment of NPD data for helicopters and UAM reference vehicles indicated that differences in the effective duration, used in the noise fraction adjustment, were both vehicle and operation dependent. This suggests that improved noise exposure estimates could be made if alternative power models were made available within AEDT. The selection of the power model for a particular vehicle/operation can be based on an analysis of the relevant NPD data set, specifically the relationship between the effective duration and observer distance. Comparisons with measured and/or simulated sound exposure data would be worthwhile to confirm this observation.

Ultimately, the AEDT aircraft mode used, i.e., fixed-wing or helicopter, will be dependent on several factors. These include what type of NPD data are provided (rarely is it the case that both fixed-wing and helicopter NPD data are specified for the same vehicle), how the takeoff and landing are modeled (with or without ground roll), and how the various other adjustments sum to produce sound exposure estimates. Limitations associated with each mode, both those identified herein with respect to the noise fraction adjustment and others in Ref. [3], indicate that modifications to the AEDT would be beneficial to the integrated noise modeling of rotary-wing vehicles.

Acknowledgments

This work was supported by the NASA Aeronautics Research Mission Directorate, Revolutionary Vertical Lift Technology Project. The authors appreciate the many helpful discussions with Kevin Shepherd, Distinguished Research Associate, at the NASA Langley Research Center.

References

[1] "Doc 9911, Recommended method for computing noise contours around airports, 2nd Edition," International Civil Aviation Organization, Montreal, Canada, 978-92-9258-360-6, 2018.

[2] "Aviation Environmental Design Tool (AEDT) Technical Manual, Version 3g," U.S. Department of Transportation, Volpe National Transportation Systems Center, Cambridge, MA, DOT-VNTSC-FAA-24-08, August 2024.

[3] Rizzi, S.A. and Rafaelof, M., "On the modeling of UAM aircraft community noise in AEDT helicopter mode," *AIAA Aviation Forum*, AIAA-2023-3363, San Diego, CA, 2023, https://doi.org/10.2514/6.2023-3363.

[4] Letica, S.J. and Rizzi, S.A., "On the modeling of urban air mobility vehicle takeoff and landing operations in the FAA Aviation Environmental Design Tool " *Noise-Con 2024*, New Orleans, LA, 2024.

[5] Lopes, L.V. and Burley, C.L., "ANOPP2 User's Manual: Version 1.2," NASA TM-2016-219342, 2016, https://ntrs.nasa.gov/citations/20160014858.

[6] Silva, C., Johnson, W.R., Solis, E., Patterson, M.D., and Antcliff, K.R., "VTOL urban air mobility concept vehicles for technology development," *AIAA Aviation Forum*, AIAA-2018-3847, Atlanta, GA, 2018, https://doi.org/10.2514/6.2018-3847.

[7] Eldred, K.M. and Miller, R.L., "Analysis of selected topics in the methodology of the Integrated Noise Model," Bolt, Beranek, and Newman, Inc., DOT-TSC-1782; BBN Report No. 4413, 1980, https://rosap.ntl.bts.gov/view/dot/9800.

[8] Watts, M.E., Greenwood, E., Smith, C.D., Snider, R., and Conner, D.A., "Maneuver acoustic flight test of the Bell 430 helicopter data report," NASA TM-2014-218266, 2014, https://ntrs.nasa.gov/citations/20140006505.

[9] Watts, M.E., Greenwood, E., Smith, C.D., and Stephenson, J.H., "Noise abatement flight test data report," NASA TM-2019-220264, 2019, https://ntrs.nasa.gov/citations/20240013572.

[10] Pascioni, K., Greenwood, E., Watts, M.E., Smith, C.D., and Stephenson, J.H., "Medium-sized helicopter abatement flight test data report," NASA TM-20210011459, 2021, https://ntrs.nasa.gov/citations/20210011459.

[11] Rizzi, S.A., Letica, S.J., Boyd Jr., D.D., and Lopes, L.V., "Prediction of noise-power-distance data for urban air mobility vehicles," *AIAA Journal of Aircraft*, Vol. 61, No. 1, 2024, pp. 166-182, https://doi.org/10.2514/1.C037435.

[12] Rizzi, S.A., Huff, D.L., Boyd Jr., D.D., Bent, P., Henderson, B.S., Pascioni, K.A., Sargent, D.C., Josephson, D.L., Marsan, M., He, H., and Snider, R., "Urban air mobility noise: Current practice, gaps, and recommendations," NASA TP-2020-5007433, October, 2020, https://ntrs.nasa.gov/citations/20205007433.

[13] "SAE AIR 1845A, Procedure for the Calculation of Airplane Noise in the Vicinity of Airports," SAE International, Warrendale, PA August 2012.

[14] "ECAC.CEAC Doc 29, Report on Standard Method of Computing Noise Contours Around Civil Airports, 4th Edition, Volume 2: Technical Guide," European Civil Aviation Conference - Conférence Européenne De L'Aviation Civile, Neuilly-sur-Seine, France, 2016.

[15] Rizzi, S.A. and Rafaelof, M., "Community noise assessment of urban air mobility vehicle operations using the FAA Aviation Environmental Design Tool," *InterNoise 2021*, Virtual Meeting, 2021, https://doi.org/10.3397/IN-2021-1482.